Calculated Transonic Flow Past Slender Fuselages and Afterbodies

MARTIN R. FINK*
United Aircraft Corporation Research Laboratories, East Hartford, Conn.

A procedure is developed for calculating the inviscid flow past slender sharp-nosed fuselages at arbitrary transonic Mach numbers. Nonaxisymmetric shapes with small camber and incidence can be represented. A revision of Spreiter and Alksne's solution for accelerating, locally near-sonic flow and an empirical description of shock wave strength and location are patched to the local linearization equations for locally subsonic and supersonic flows. The local linearization method and the transonic method of Oswatitsch are applied to calculation of flow past converging afterbodies downstream of semi-infinite cylinders at low supersonic Mach numbers down to one. Calculated pressure distributions are in good agreement with data.

Nomenclature

A = function of forebody or afterbody shape and fineness ratio
C_D = drag coefficient, nondimensional with respect to S_{max}
C_P = pressure coefficient, $2(P - P_1)/(\gamma P_1 M^2)$ or $-2u - (r')^2$
C = Euler's constant (0.5772 . . .)
e = base of Naperian logarithms
f_H = nondimensional axial perturbation velocity calculated from linearized supersonic theory for a freestream Mach number of $(2)^{1/2}$
G = term in the differential equation for accelerating transonic flow, corresponding to the triple integral in Eq. (49) of (2)
M = freestream Mach number
P = static pressure
r = local radius, nondimensionalized with respect to length
S = local nondimensional cross-section area, πr^2
u = nondimensional axial perturbation velocity
x = local distance from upstream end of configuration, nondimensionalized with respect to length
α = angle of attack, rad
γ = specific heat ratio, taken as 1.4
λ = ratio of ellipse major axis to minor axis
ξ = transonic Mach number similarity parameter
τ = ratio of maximum diameter to length, $2r_{max}$
ϕ = nondimensional perturbation velocity potential
Φ = aximuth angle, measured from lateral direction leeward, deg

Subscripts

B = evaluated at the base
i = evaluated from linearized incompressible theory
max = maximum
$M = 1$ = evaluated at a Mach number of one
r,rr = first and second derivatives with respect to r
x,xx = first and second derivatives with respect to x
1 = evaluated at freestream static conditions
2 = evaluated downstream of a shock wave

Superscripts

$',\,'',\,'''$ = first, second, and third derivatives with respect to x

Introduction

WHEN accelerating through transonic speeds, aircraft must change the exit geometry of the propulsive-system exhaust nozzle in order to keep the pressure drag acceptably small. Thus, one must be able to predict detailed variations of local flow properties along the aft fuselage with flight Mach number. This information also is needed for the design of ejector blow-in doors and nozzle external surfaces. For prediction of fuselage transonic drag rise and of interactions between the airframe and propulsive system, it was necessary to develop an empirical method for predicting pressure distributions on slender fuselages and nacelles throughout the transonic regime.

One type of analytical method, originated by Oswatitsch and Keune,[1] simplifies the axisymmetric transonic-flow differential equation by assuming that the axial velocity gradient is positive and relatively constant. The predicted flow is in good agreement with the data for forebodies, where this assumption is valid. Poor agreement occurs for the aft part of fuselages, where the axial velocity gradient is nonconstant and generally negative. A more promising approach seemed to be that of Spreiter and Alksne,[2] who used different assumptions in different axial regions. Results for these regions are patched such that the velocity and its first derivative are continuous. Their transonic method gives good agreement with data at Mach numbers very near one and poor agreement at other transonic speeds. Changes were needed to provide reasonable predictions near the high and low ends of the transonic regime while retaining the previous good agreement at near-sonic speeds.

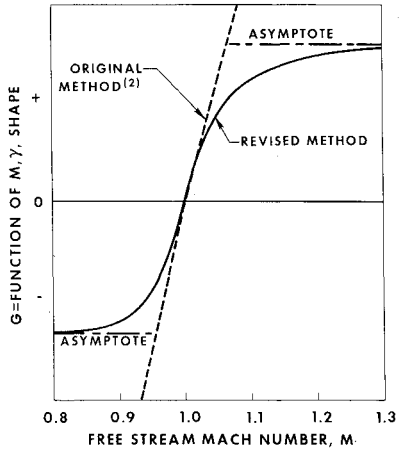

Fig. 1 Variation of the function G with Mach number.

Presented as Paper 70-556 at the AIAA Atmospheric Flight Mechanics Conference, Tullahoma, Tenn., May 13–15, 1970; submitted May 26, 1970; revision received September 24, 1970.

* Senior Consulting Engineer, Aerodynamics. Associate Fellow AIAA.

Transonic flow past a slender nonaxisymmetric lifting fuselage can be analyzed by superimposing results for several simpler flows.[3] One is the axisymmetric flow past the area-equivalent body of revolution at the correct Mach number and specific-heat ratio. The others, in the cross-flow plane, are added to that solution to yield the effects of noncircular cross section and of small camber and incidence. These latter solutions can be obtained by existing techniques. To first order, a transonic solution for axisymmetric flow can therefore be applied to calculation of flow past realistic nonaxisymmetric lifting fuselages.

The objective of this study was the development of an analytic method for prediction of static pressure distributions on fuselages and nacelle afterbodies at arbitrary transonic Mach numbers.

Development of Calculation Method

Equations for Velocity Gradient

The nondimensional small disturbance differential equation for axisymmetric transonic flow is

$$(1 - M^2)\phi_{xx} + \phi_{rr} + \phi_r/r = (\gamma + 1)M^2\phi_x\phi_{xx} \quad (1)$$

which contains a nonlinear term as its right-hand side. One way in which this term can be made linear is to assume that the nondimensional axial perturbation velocity $u = \phi_x$ is relatively constant over some local region. When the local axial component of Mach number is subsonic, the local linearization method[2] then yields

$$(du/dx)_{\text{SUB}} = (S'''/4\pi)\ln[1 - M^2 - (\gamma + 1)M^2u] + du_i/dx \quad (2)$$

where u_i is the nondimensional axial perturbation velocity in linearized incompressible flow.

When the local axial component of Mach number is supersonic, the local linearization equation[2] is

$$(du/dx)_{\text{SUPER}} = (S'''/4\pi)\ln[M^2 - 1 + (\gamma + 1)M^2u] + df_H/dx \quad (3)$$

where f_H is the nondimensional axial perturbation velocity in linearized supersonic flow at a freestream Mach number equal to the square root of two. Both Eq. (2) and Eq. (3) have a logarithmic singularity when $u = (M^2 - 1)/[(\gamma + 1)M^2]$ which occurs when the local axial component of Mach number is equal to one.

The nondimensional velocities given by linearized subsonic and supersonic theories are independent of Mach number at the axial location where S'' is equal to zero. Thus, velocity distributions on axisymmetric fuselages in fully subsonic or fully supersonic flow can be calculated[2] by numerically integrating Eq. (2) or Eq. (3), with the velocity at that point taken as the starting condition.

For a locally near-sonic accelerating flow, the nondimensional axial velocity gradient $du/dx = \phi_{xx}$ on the right-hand side of Eq. (1) is assumed relatively constant. After considerable manipulation, Eq. (53b) of Ref. 2 is obtained. This equation can be simplified and re-written as

$$(du/dx)_{\text{TRANS}} = (S'S''/4\pi S) + \{2/[(\gamma + 1)M^2re^G]\} \times \exp[(4\pi/S'')(u + G - f_H/2)] \quad (4)$$

in which the term G was evaluated in Ref. 2 as

$$G(M,\gamma) = (M^2 - 1)/[(\gamma + 1)M^2] \quad (5)$$

To obtain a finite velocity gradient at the point where S'' is equal to zero, it is necessary to assume that

$$(u)_{S''=0} = \tfrac{1}{2}(f_H)_{S''=0} - G \quad (6)$$

As with the local linearization method for fully subsonic and supersonic flows, the value of u at this axial station then serves as the starting condition for numerical integration. At this station, Eq. (4) becomes

$$(du/dx)_{S''=0} - (S'''/4\pi)\ln(du/dx)_{S''=0} = \tfrac{1}{2}(df_H/dx)_{S''=0} + (S'''/4\pi)\ln[(\gamma + 1)M^2re^G/2] \quad (7)$$

from which the velocity gradient at the starting point is computed.

The term G arises from a complicated integral within Eq. (49) of Ref. 2. It was evaluated therein by use of approximations valid only for Mach numbers very close to one. Agreement between calculated results and data is best at a Mach number of one, where G is zero, and becomes poor as G increases in magnitude. If a revised solution is to be meaningful at high transonic speeds, G should approach $-\frac{1}{2}(f_H)_{S''=0}$ with increasing M so that the velocity given by Eq. (6) would approach that of linearized supersonic theory. Similarly, G should approach $-(u_i)_{S''=0} + \frac{1}{2}(f_H)_{S''=0}$ with decreasing transonic Mach number. This required asymptotic behavior near Mach 1 and at the high and low ends of the transonic regime is sketched in Fig. 1. Very near a Mach number of one, G depends on M and γ and is independent of body shape. Away from Mach one, G depends on body shape, is inversely proportional to fineness ratio squared, and is independent of M and γ. The simplest function which has this behavior is

$$M \leq 1,\ G = \tfrac{1}{2}(f_H - 2u_i)_{S''=0}\{1 - \exp[-\xi/(f_H/2\tau^2 - u_i/\tau^2)_{S''=0}]\} \quad (8)$$

$$M \geq 1,\quad G = -\tfrac{1}{2}(f_H)_{S''=0}\{1 - \exp[\xi/(fH/2\tau^2)_{S''=0}]\} \quad (9)$$

where the transonic Mach number similarity parameter ξ is defined by

$$\xi = (M^2 - 1)/[(\gamma + 1)M^2\tau^2] \quad (10)$$

The function G as given by Eq. (5) forces the velocity at the starting point, given by Eq. (6), to satisfy the Mach number independence principle. This principle states that the axial distribution of local Mach number is approximately independent of transonic freestream Mach number. From Eqs. (8) and (9), this principle is approximately satisfied only for $-1 < \xi < 1$.

The previous equations for G could be used directly in the local linearization method.[2] If this were done, a region of locally supersonic flow having moderate axial extent would be predicted at Mach numbers infinitesimally above the lower critical Mach number. This supersonic region would terminate in a gradual recompression with a logarithmically infinite slope at its sonic point. The resulting calculated pressure distribution and pressure drag would change discontinuously at the lower critical Mach number. That behavior does not occur in a real flow. Instead, the locally supersonic region should be ended by a shock wave which smoothly moves downstream from the high subsonic minimum pressure location as Mach number is increased above its lower critical value.

Empirical Approximations for Shock Wave

At a freestream Mach number of one, a simple prediction of shock wave location was obtained. The shock wave is assumed to be at the afterbody location at which S'' is equal to zero. It can be shown that this location is slightly upstream of that determined by Hosokawa.[4] Empirically, this predicted location is downstream of shock wave locations measured in both slotted-wall and perforated-wall wind tunnels. Attempts to derive an analytical proof of this assumed shock wave location in axisymmetric flow were unsuccessful. However, it was shown by Truitt[5] that for a Mach number of one, the shock wave occurs on the surface of a two-dimensional airfoil at the location where the second derivative of body shape is equal to zero, i.e., at an area-

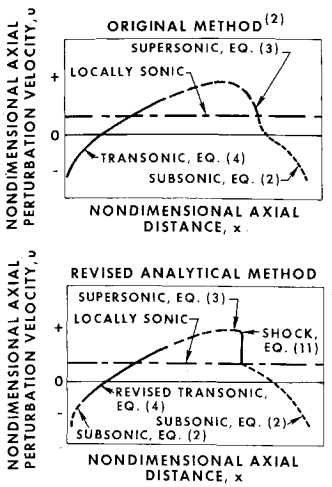

Fig. 2 Calculation of fuselage transonic velocity distributions by switching to different equations: parabolic arc bodies of revolution.

distribution inflection point. From inspection of measured variations of shock wave location with low transonic Mach number, it was arbitrarily assumed that the shock wave location varied linearly with transonic Mach number similarity parameter ξ. Its position is then determined as a linear variation from the minimum-pressure location at the lower critical similarity parameter through the described position at $\xi = 0(M = 1)$. Shock wave locations estimated in this manner seem to be upstream of those predicted by Hosokawa's method[4] throughout the transonic regime. At some Mach number greater than one, the shock wave location predicted in this manner will have moved downstream to a position at which smooth supersonic recompression to a local axial Mach number of one is calculated from Eq. (3). Above that Mach number, that type of recompression[2] is used instead of a discrete shock wave.

Shock wave strength at the surface should be determined by a method which includes strong viscous interactions between the boundary layer and shock wave.[6] Rigorous inviscid solutions have a normal shock wave immediately followed by a strong subsonic expansion.[4,7] A correlation of shock strengths measured on two-dimensional airfoils[7] was closely approximated by an oblique shock which has a downstream Mach number of one. For convenience in the computation procedure, the shock wave was arbitrarily assumed to produce a downstream axial component of Mach number equal to 0.999 rather than unity. Thus, the axial perturbation velocity downstream of the shock wave was empirically taken as

$$u_2 = (0.999 - M^2)/[(\gamma + 1)M^2] \qquad (11)$$

These crude approximations to shock wave location and strength are interrelated. In some mathematically rigorous solutions the calculated shock wave is too strong at a given axial location, or too far forward with a given assumed shock-strength mechanism. The calculated recompression then is too strong and the predicted pressure drag is too small. It is easy to devise analytical methods which yield pressure distributions having plausible shapes; it is difficult to devise methods which do not predict negative pressure drags at low transonic Mach numbers. The simple approximate empirical method described herein gave positive transonic pressure drags for all fuselage shapes analyzed. Other approximations, which at first glance seemed more rational, gave negative pressure drags as the Mach number was increased above its lower critical value.

Patching Procedure

The computation procedure originally used with the local linearization method for transonic speeds[2] is sketched in the upper part of Fig. 2. The forward part of the velocity distribution was determined by numerical integration of Eq. (4). Beyond the sonic point, the numerical integration switched to Eq. (3) when that equation gave a smaller velocity gradient than did Eq. (4). Thus the results of the transonic and supersonic equations were patched with continuous velocity and continuous velocity gradient. Calculations continued with Eq. (3) until recompression through a local axial Mach number of one was predicted, with a very large negative velocity gradient. The computation then switched to Eq. (2) for subsonic local linearization.

In the revised method, starting conditions are obtained from Eq. (6) with G defined by Eq. (8) or Eq. (9). The velocity gradient calculated from Eq. (7) is compared with that from Eq. (2) or Eq. (3) depending on whether the local axial velocity is subsonic or supersonic. The equation which gives the smaller velocity gradient is used, so the logarithmic singularity in Eqs. (2) and (3) is avoided. As sketched in the lower part of Fig. 2, the calculations may use subsonic local linearization, patch into transonic accelerating flow and then into supersonic local linearization with increasing downstream distance. Deceleration to subsonic flow and the subsonic local linearization equation occurs either through a shock wave whose strength is defined by Eq. (11) or from smooth deceleration of the calculated supersonic flow, whichever is calculated to occur first. Bumpy area distributions are acceptable as long as the second derivative of cross section area is continuous. The calculations then must be started at the most forward location at which S'' is equal to zero.

Radial attenuation of the flow perturbation generated by the fuselage can be calculated by use of conventional slender-body theory. Validity of this procedure has been verified experimentally[8] for fuselages at transonic Mach numbers.

Calculated Trends for Fuselages

Calculated pressure distributions are available[2] for a fineness ratio 10 parabolic arc body of revolution at Mach numbers of 0.935 (wholly subsonic), 1.00, and 1.21 (wholly supersonic axial component of velocity). Pressure distributions for those three Mach numbers and for Mach numbers of 0.975 and 1.05 as calculated by the method described herein are shown in Fig. 3. The curves for the highest and lowest Mach numbers were essentially identical to the earlier results;[2] that for a Mach number of one agreed with those re-

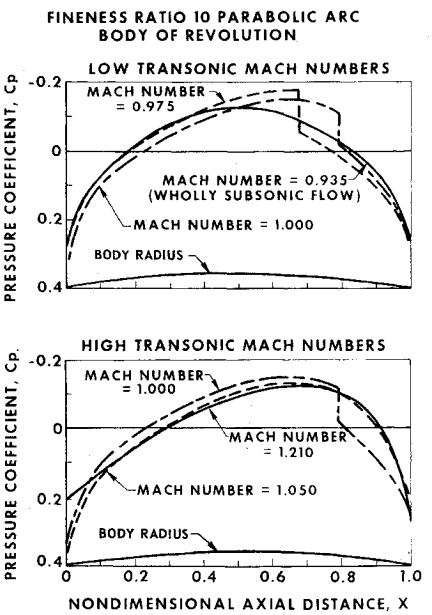

Fig. 3 Pressure distributions at different transonic Mach numbers.

sults at locations upstream of the shock wave. As the Mach number is increased through the transonic regime, the easily inferred trends are; 1) growth of a region of locally supersonic flow ended by a shock wave, with small changes in pressure coefficient on the forebody; 2) relatively uniform positive shift of pressure coefficient upstream of the shock wave as the Mach number is increased through one; and 3) adjustment of the pressure distribution near the apex as the subsonic stagnation-point flow becomes a supersonic conical flow.

The calculated variation of pressure drag similarity parameter C_D/τ^2 with the transonic Mach number similarity parameter ξ is shown in Fig. 4 for parabolic arc bodies of revolution with fineness ratios of $6(2)^{1/2}$ and 10. Separate curves are shown for the forward half of the body and the complete body. These parameters correlate only the results for supersonic Mach numbers (positive ξ) because the lower critical Mach number does not correlate with ξ. Results for the forward half are in good agreement with previous results[2] for a Mach number of one and for fully supersonic flow. Near a Mach number of one, they approximately satisfy the Mach number independence principle.

$$(dC_D/dM)_{M=1} = [2/(\gamma + 1)][2S_B/S_{\max} - (C_D)_{M=1}] \quad (12)$$

The drag coefficient of the complete sharp-base fuselage at a Mach number of one, as calculated by the method described herein, is about $\frac{2}{3}$ of the earlier value.[2] Contrary to the prediction obtained from Eq. (12), the slope of the fuselage drag curve is positive rather than negative. Aft movement of the fuselage shock wave as the Mach number is increased through one causes this disagreement with the Mach number independence principle. Calculations also were conducted by the method developed herein but with gradual supersonic recompression rather than a shock wave. As can be seen in Fig. 7, those drag coefficients do agree with those of Spreiter and Alksne[2] for a Mach number of one and the slope does agree with Eq. (12).

As is predicted by linearized supersonic theory, the pressure drag of the rearward half of this fuselage shape at very low supersonic speeds is more than 25% larger than that of the front half (Fig. 4). Changes in afterbody pressure distribution caused by variable-geometry portions of the engine exhaust nozzle therefore can affect a relatively large fraction of the fuselage transonic pressure drag.

Comparisons with Fuselage Data

Parabolic Arc Body of Revolution

Transonic pressure distributions calculated for a fineness ratio 10 parabolic arc body of revolution are compared in Fig. 5 with data[8] for high subsonic Mach numbers up to one. These calculations were conducted for a sharp-base fuselage

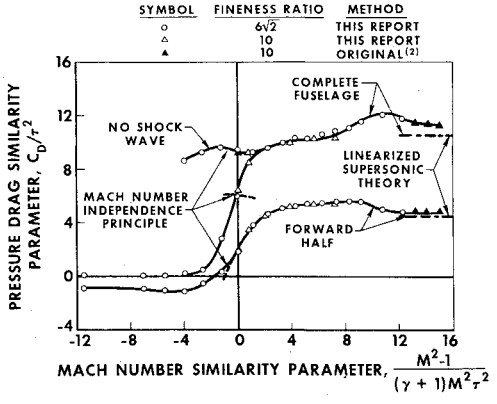

Fig. 4 Variation of pressure drag similarity parameter with Mach number similarity parameter.

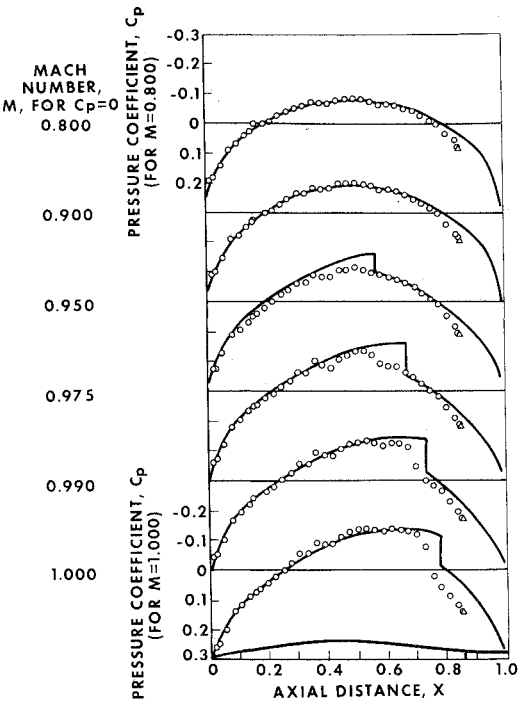

Fig. 5 Computed and measured pressure distributions for fineness ratio 10 parabolic arc body of revolution at low transonic speeds.

rather than the sting-supported model shape sketched at the bottom of the figure. Pressure distributions at the subcritical Mach numbers of 0.80 and 0.90 are closely predicted except for effects of the support sting at 85% of the nominal model length. A small supersonic expansion followed by a shock wave was computed for a Mach number of 0.95; the data show less supersonic expansion and no discrete shock wave. This difference is consistent with calculated transonic viscous effects.[6] At a Mach number of 0.975 the measured forebody pressures are closely predicted. The measured recompression was that of a lambda shock with its aft leg near the predicted shock location. At both of these Mach numbers the measured pressure distributions downstream of the shock wave were well predicted.

The pressure distribution on the forward $\frac{2}{3}$ of the fuselage was closely predicted at a Mach number of 0.99. At this test condition the Mach number similarity parameter was -0.83, and the change in pressure distribution between this Mach number and 1.00 satisfies the Mach number independence principle. The measured shock wave location moved aft with this increase of Mach number, contrary to the lack of motion predicted by the independence principle. Data for a fineness ratio 14 parabolic arc body at Mach numbers of 0.99, 1.00, and 1.01,[8] not shown here, did not satisfy the Mach number independence principle because the corresponding increments of similarity parameter (1.6) were too large. Data from the aft part of the model at these test conditions was influenced by reflection of forebody expansion waves from the tunnel walls to the afterbody as compression waves.[9]

A similar comparison with data for this model at supersonic Mach numbers down to 1.01 is given in Fig. 6. Measured and calculated pressure distributions at that lowest Mach number are in good agreement. Ahead of 70% length, they agree with the Mach number independence principle applied to the Mach 1.00 results. At Mach numbers of 1.01–1.075 nearly all fuselage data obtained in this test facility[8,10,11] were influenced by reflection of the bow shock wave from the tunnel walls onto the models. This reflection occurred as an expansion region at the lowest supersonic Mach numbers and as a weak compression followed by weak

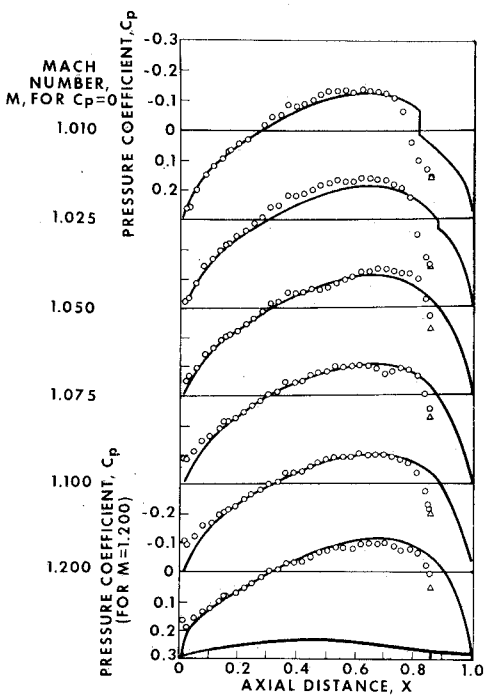

Fig. 6 Computed and measured pressure distributions for fineness ratio 10 parabolic arc body of revolution at high transonic speeds.

expansion at 1.05 and 1.075. Except for these irregularities in the data, the agreement is good at Mach numbers up to 1.05. For these Mach numbers, the bow shock wave was detached and no other analytical method would be expected to apply.

Calculations do not agree with the data near the apex at Mach numbers from 1.075 to 1.20. The actual bow shock wave was attached at the apex, followed by locally subsonic conical flow at Mach numbers of 1.075 and 1.10 and by locally supersonic flow at freestream Mach numbers above 1.14. However, if the axial component of Mach number at the apex is not supersonic, the analytical method used herein yields an approximation to subsonic stagnation-point flow. This discrepancy could be removed by smoothly fairing the calculated curves into tabulated results for attached conical flow.

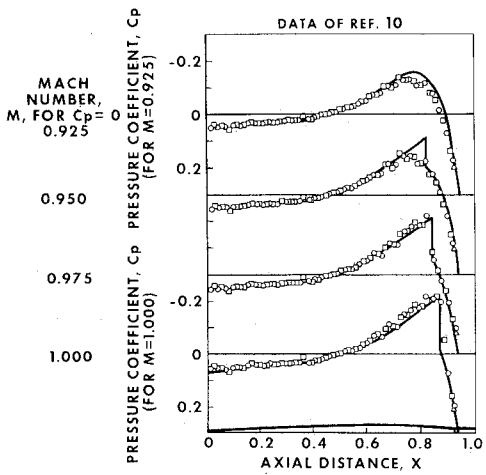

Fig. 7 Computed and measured pressure distributions for body with maximum diameter at 70% of length at low transonic speeds.

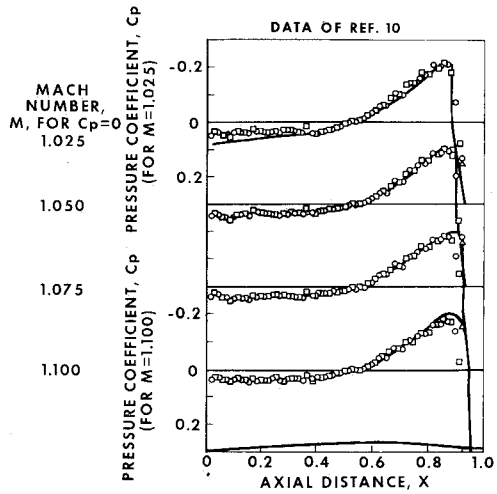

Fig. 8 Computed and measured pressure distributions for body with maximum diameter at 70% of length at high transonic speeds.

Other Axisymmetric Bodies

Measured transonic pressure distributions are available[10] for a series of five axisymmetric bodies with a fineness ratio of 12 and differing axial locations of maximum diameter. A comparison with calculated values for the body with maximum diameter at 70% of its length (the most rearward location) is given in Figs. 7 and 8. At Mach numbers up to one (Fig. 7), agreement is very good except that the data did not have the strong predicted supersonic expansion just ahead of the shock wave at a Mach number of 0.95. This expansion did occur at Mach numbers of 0.975 and 1.00. In particular, there is good agreement downstream of the shock wave despite the admittedly crude representation of shock wave location and strength. Agreement remains very good at supersonic speeds (Figs. 8) except for the expected error near the apex at a Mach number of 1.025.

A similar comparison is given in Figs. 9 and 10 for the body with the most forward (30%) location of maximum diameter. Analytically, this body shape is the mirror image of that for Figs. 7 and 8 so the calculated pressure distributions in fully subsonic flow were mirror images. The general agreement at Mach numbers up to one (Fig. 9) is good, except for the shock wave location. This difference is in the direction expected for wind-tunnel wave reflection effects.[9] At

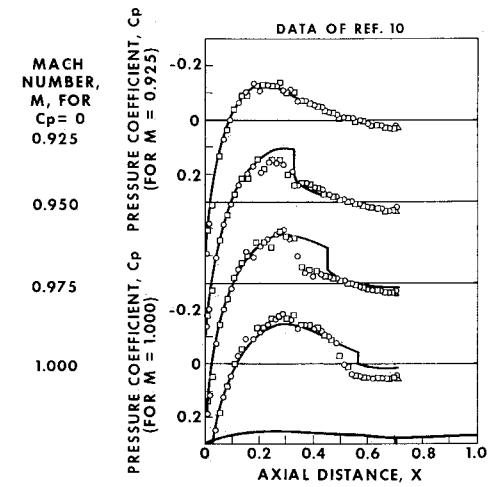

Fig. 9 Computed and measured pressure distributions for body with maximum diameter at 30% of length at low transonic speeds.

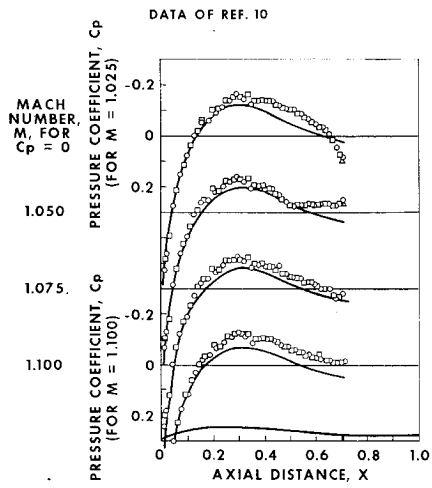

Fig. 10 Computed and measured pressure distributions for body with maximum diameter at 30% of length at high transonic speeds.

low supersonic Mach numbers (Fig. 10) the calculated curves have the correct trend. Over the forward 10% of the body, however, their level was too positive. The bow shock wave was detached and may have been reflected from the tunnel walls onto the model as an expansion region, leading to this discrepancy.

Nonaxisymmetric Lifting Bodies

Perturbation velocities on nonaxisymmetric lifting slender bodies are given to first order[3] as the sum of those for 1) the nonlifting area-equivalent body of revolution at the free-stream Mach number and specific-heat ratio, as can be estimated by the method described herein, plus 2) the radial and aximuthal velocities produced in the incompressible crossflow plane by axial area growth of the nonaxisymmetric cross section, minus 3) the radial velocity in the cross-flow plane caused by axial area growth of the area-equivalent body of revolution, plus 4) the radial and azimuthal velocities produced in the crossflow plane by translatory motion of the actual cross section due to camber and incidence. That is, the effects of camber, incidence, and noncircular cross section as determined for incompressible flow can be added to the effects of subsonic, transonic, and moderate supersonic Mach number. Data are available[11] for a series of bodies with the area distribution of a fineness ratio 12 parabolic arc body of revolution but with ellipse cross sections. A comparison between measured and calculated pressure distributions along five meridian lines is given in Fig. 11 for the body with an axis ratio λ of 3 at 4° angle of attack and a Mach

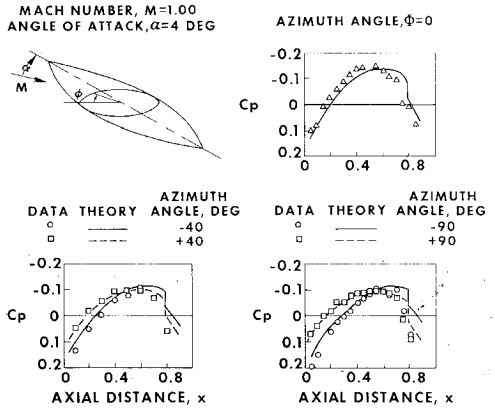

Fig. 11 Axial pressure distributions at different azimuth angles.

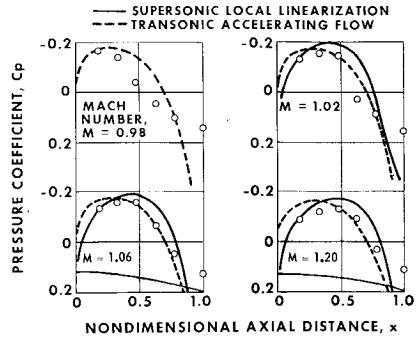

Fig. 12 Comparison of theories with data for parabolic arc afterbody of fineness ratio 3.33.

number of one. The calculated effects of incidence include the $-(\lambda \sin\alpha \cos\Phi)^2$ term which is of second order in angle of attack but cannot be neglected. The pressure distributions on the lateral meridian ($\Phi = 0$) generally agree except near the measured lambda shock. At the other azimuth angles, good agreement also was obtained except near the shock wave and the support sting.

Calculated Trends for Forebodies and Afterbodies

The subsonic local linearization method[2] gave good results when used for subcritical flow past slender smooth fuselages having pointed apexes and bases. When applied to sharp-apex forebodies followed by semi-infinite cylinders, the calculated pressure distributions looked reasonable. However, the predicted pressure drag coefficients became increasingly negative with increasing subcritical Mach number. For a fineness ratio 5 parabolic arc forebody, the negative drag coefficient calculated at the critical Mach number is about 40% of the positive drag coefficient at Mach one. This physically impossible result of nonzero pressure drag in inviscid subcritical nonlifting flow is caused by the original assumption[2] that the starting condition for numerical integration of Eq. (2) can be obtained from linearized subsonic theory. An order-of-magnitude analysis of the effect of the nonlinear term of Eq. (1), accompanied by trial-and-error substitution in numerical calculations, had led to a revised starting condition. The correct starting axial perturbation velocity, specified at the starting location where $S'' = 0$ for Mach numbers less than the lower critical Mach number, should be given by

$$(u)_{S''=0} = (u_i)_{S''=0} \exp(-A/\xi) \tag{13}$$

where A is a positive number of order unity which depends on both forebody shape and fineness ratio. For transonic flow with the starting condition given by Eq. (6) the term G must be slightly revised from that given by Eq. (8) and sketched in Fig. 1. The resulting small correction at sub-

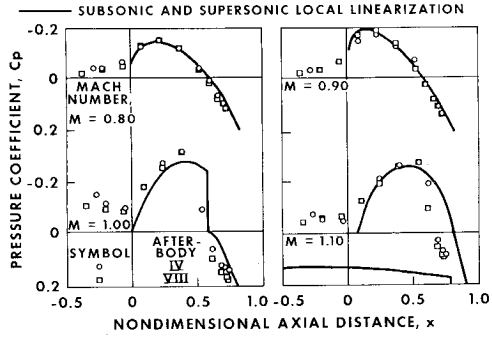

Fig. 13 Computed and measured pressure distributions for blunt base afterbodies with exhaust flow.

sonic speeds reduces the calculated perturbation velocities, slightly raises the critical Mach number, and provides zero pressure drag in fully subsonic flow. The inviscid pressure distribution on a sharp-base afterbody downstream of a semi-infinite cylinder in fully subsonic flow is a mirror image of the corresponding forebody flow.

At high transonic Mach numbers down to one, the flow past an afterbody can be regarded as an initial expansion caused by decrease of surface slope followed by gradual compression caused by streamline convergence. Thus the average local Mach number everywhere except near a sharp base would be larger than the freestream Mach number. The supersonic local linearization relation, Eq. (3), then is directly applicable. Computation would start at the point on the afterbody at which S'' is equal to zero, and the perturbation velocity at that point would be equal to f_H. This method yields a logarithmic singularity at the afterbody shoulder, as does linearized supersonic theory. Calculated curves should be arbitrarily faired to zero pressure coefficient at the shoulder.

Another analytical method for calculating transonic flow past afterbodies can be obtained by direct application of the early solution of Oswatitsch and Keune[1] for the parabolic partial differential equation for accelerating transonic flow. After manipulation, that transonic theory yields

$$u = f_H/2 + (S''/4\pi) \ln[(\gamma + 1)\pi M^2 \tau^2 r e^C/4] \qquad (14)$$

as a direct prediction of perturbation velocity. Of course, Eq. (14) would be expected to apply only for afterbody shapes which have accelerating flow along most of their length. It can be shown that if an afterbody has zero slope at its shoulder and a sharp base, the pressure drag coefficient at a Mach number of one is predicted from Eq. (14) to be half that given by linearized supersonic slender-body theory. This result also applies for the mirror-image forebody, and as can be seen from Fig. 4 it provides a reasonable though not exact estimate.

Pressure distributions calculated by separate use of Eq. (14) for transonic accelerating flow and Eq. (4) for supersonic local linearization are compared in Fig. 12 with transonic data[12] for a sharp-base parabolic arc afterbody with maximum diameter 0.3 times its length. Although the assumption of constant positive velocity gradient is poor for this shape, Eq. (14) was in qualitative agreement with the data for Mach numbers near one. It failed to predict the decrease of intensity of the initial expansion, and aft movement of minimum-pressure region, with increasing supersonic Mach number. These trends were correctly predicted by supersonic local linearization although the magnitude of minimum pressure was overestimated.

Data for a blunt-base afterbody with a low-pressure-ratio cold exhaust jet and nearly parabolic arc contour[13] are compared in Fig. 13 with subsonic local linearization for subcritical Mach numbers of 0.8 and 0.9 and supersonic local linearization for Mach numbers of 1.0 and 1.1. The calculations were performed for a sharp-base afterbody and the effect of the exhaust jet at 74% of the ideal length was neglected. For a Mach number of 1.0, a shock wave with strength given by Eq. (11) was arbitrarily inserted at $x = 0.577$, where S'' equalled zero. The flow downstream of this shock was given by subsonic local linearization. Afterbodies IV and VIII[13] had identical converging regions preceded by different cylinder lengths. Lack of major differences between the two sets of data illustrates that viscous effects were not large. At a Mach number of 1.10 the observed shock wave is a lambda shock at the exhaust jet. Agreement between the afterbody data and the local linearization theories is good at all four Mach numbers, except near the shock wave. The methods described herein give useful predictions of afterbody pressure distributions at subsonic Mach numbers up to the critical Mach number and low supersonic Mach numbers down to one.

References

[1] Oswatitsch, K. and Keune, F., "The Flow Around Bodies of Revolution at Mach Number One," *Proceedings of the Conference on High-Speed Aeronautics*, Polytechnic Institute of Brooklyn, June 20–22, 1955, pp. 113–131.

[2] Spreiter, J. R. and Alksne, A. Y., "Slender-Body Theory Based on Approximate Solution of the Transonic Flow Equation," TR R-2, 1959, NASA.

[3] Heaslet, M. A. and Spreiter, J. R., "Three-Dimensional Transonic Flow Theory Applied to Slender Wings and Bodies," Rept., 1318, 1957, NACA.

[4] Hosokawa, I., "A Refinement of the Linearized Transonic Flow," *Journal of the Physical Society of Japan*, Vol. 15, No. 1, Jan. 1960, pp. 149–157.

[5] Truitt, R. W., "Shockless Transonic Airfoils," AIAA Paper 70-187, New York, 1970.

[6] Sichel, M., "Theory of Viscous Transonic Flow—A Survey," Paper 10, *Transonic Aerodynamics*, AGARD Conference Proceedings 35, Sept. 1968.

[7] Sinnott, C. S., "On the Prediction of Mixed Subsonic/Supersonic Pressure Distributions," *Journal of the Aerospace Sciences*, Vol. 27, No. 10, Oct. 1960, pp. 767–778.

[8] Taylor, R. A. and McDevitt, J. B., "Pressure Distributions at Transonic Speeds for Parabolic-Arc Bodies of Revolution Having Fineness Ratios of 10, 12, and 14," TN 4234, March 1958, NACA.

[9] Spreiter, J. R., Smith, D. W., and Hyett, B. J., "A Study of the Simulation of Flow with Free-Stream Mach Number 1 in a Choked Wind Tunnel," TR R-73, 1960, NASA.

[10] McDevitt, J. B. and Taylor, R. A., "Pressure Distributions at Transonic Speeds for Slender Bodies Having Various Axial Locations of Maximum Diameter," TN 4280, July 1958, NACA.

[11] McDevitt, J. B. and Taylor, R. A., "Force and Pressure Measurements at Transonic Speeds for Several Bodies Having Elliptical Cross Sections," TN 4362, Sept. 1958, NACA.

[12] Kurn, A. G., "Drag Measurements on a Series of Afterbodies at Transonic Speeds Showing the Effect of Sting Interference," C.P. 984, Sept. 1966, Aeronautical Research Council, Great Britain.

[13] Henry, B. Z., Jr. and Cahn, M. S., "Pressure Distributions Over a Series of Related Afterbody Shapes as Affected by a Propulsive Jet at Transonic Speeds," RM L56K05, Jan. 1957, NACA.